Spectrochimica Acta Part A: Molecular and Biomolecular Spectroscopy 320 (2024) 124593

Contents lists available at ScienceDirect

Spectrochimica Acta Part A: Molecular and Biomolecular Spectroscopy

journal homepage: www.journals.elsevier.com/spectrochimica-acta-part-a-molecular-and-biomolecular-spectroscopy

How deprotonation of cohumulone and colupulone influence their UV/Vis and CD spectrum

Anja Petek [a], Urban Bren [a,b,c], Gregor Hostnik [a,*]

[a] Faculty of Chemistry and Chemical Technology, University of Maribor, Smetanova ulica 17, SI-2000, Maribor, Slovenia
[b] Faculty of Mathematics, Natural Sciences and Information Technologies, University of Primorska, Glagoljaška ulica 8, SI-6000, Koper, Slovenia
[c] Institute of Environmental Protection and Sensors, Beloruska ulica 7, SI-2000, Maribor, Slovenia

HIGHLIGHTS

- Cohumulone and colupulone are important hops (*humulus lupulus*) constituents.
- The pH dependence of studied compounds' UV/vis spectrum.
- TD-DFT provides information on electronic transitions resulting in the spectra.
- The deprotonation positions of compounds and the absolute configuration of cohumulone.

GRAPHICAL ABSTRACT

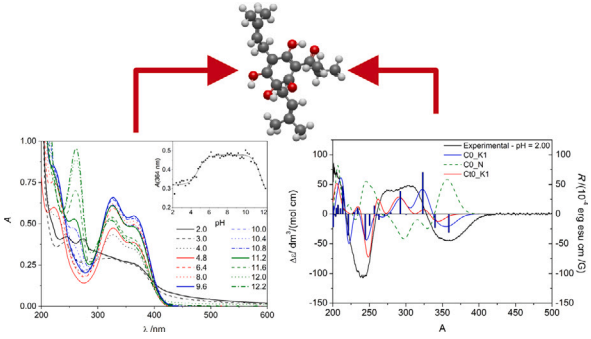

ARTICLE INFO

Keywords:
Cohumulone
Colupulone
UV/Vis spectrum
CD-spectrum
TD-DFT
Absolute configuration

ABSTRACT

Cohumulone and colupulone are representatives of α- and β-acids, respectively. These compounds are important antimicrobial hop (*Humulus lupulus*) constituents, where cohumulone is an important source of the bitter taste of beer. In this study, we examined the pH dependence of UV/Vis spectra of both compounds while CD spectra of cohumulone were also measured at various wavelengths. This facilitated the examination of the protolytic equilibrium of both compounds, where the second pK_a value of cohumulone was determined for the first time. Additionally, comparing experimental spectra with spectra calculated using time-dependent density functional theory (TD-DFT) enabled the determination of the most likely deprotonation positions and corresponding species most likely present in the aqueous solution at various pH values. Last but not least, comparing calculated and experimental CD spectra of cohumulone facilitated the determination of the absolute stereoconfiguration of cohumulone.

1. Introduction

The plant of *Humulus lupulus* is well-known worldwide as the raw material in the brewing industry. Therefore, it represents a high-value crop grown worldwide for application in the brewing industry. Female plants are cultivated for their inflorescence (hop cones or "hops"), which contain large quantities of terpenes and bitter acids in extracellular trichomes known as lupulin [1]. Hops are widely used to preserve beer and to give it a characteristic aroma and flavour.

Humulus lupulus has been attributed anti-inflammatory and antimicrobial properties, as well as diuretic, digestive, sedative and progestogenic properties [2]. For this wide range of health benefits, it has even been regarded as a life-prolonging plant [3].

* Corresponding author.
E-mail addresses: anja.petek@um.si (A. Petek), urban.bren@um.si (U. Bren), gregor.hostnik@um.si (G. Hostnik).

https://doi.org/10.1016/j.saa.2024.124593
Received 29 March 2024; Received in revised form 22 May 2024; Accepted 2 June 2024
Available online 7 June 2024

Among its compounds present in beer, terpenes and their oxidation products impart aroma to finished beer, while the bitter acids (α- and β-acids) represent precursors for compounds responsible for beer's distinctive bitter taste [4]. Based on the content of these compounds, hop species are traditionally divided into two categories: bittering hops with high α-acid contents and aroma hops, which impart volatile terpenes with favourable aromas. Some hop varieties can be applied for both purposes [5].

During the brewing process the α-acids are converted into iso-α-acids, which impart the typical bitter taste to the beer; the β-acids, however, decompose and do not add anything to the taste of the final product [6,7]. The α-acids consist of a series of closely related analogues differing only in the acyl side chain [8]; the major compounds include cohumulone, humulone and adhumulone. These compounds represent also the more important constituents of hop extracts from the brewer's point of view [9]. Therefore, it is important for brewers to know the α-acid content of the extracts that they buy, and large economic interests are served with an unambiguous quantification of the α-acids, as their content mainly determines the price of hop products [10].

The most important chemical conversion occurring during wort boiling is the thermal isomerization of the α-acids into the bitter-tasting iso-α-acids via the acyloin-type ring contraction [8]. This isomerization of represents the most technologically important reaction of hops because iso-α-acids are largely responsible for the very characteristic beer bitterness. Because there are three main α-acids present in hops, six major iso-α-acids are formed in beer, i.e., the trans- and cis-isomers of isocohumulone, isohumulone, and isoadhumulone [11]. Successful isomerization of α-acids is of crucial importance for proper bear taste. At the origin of the poor α-acid isomerization are the limited solubility of α-acids in the wort, incomplete isomerization during the boil, and depletion of α-acids or iso-α-acids because of adsorption on the trub being formed [8]. Moreover, factors such as pH, wort gravity, hopping rate, hop product(s) used, presence of divalent cations, duration and temperature of the boil, as well as the degree of dispersion of the α-acids upon the addition of hops all exert significant influences on the α-acid isomerization yield and final utilization [12–14]. Furthermore, the reaction of isomerization is strongly affected by the protolytic equilibrium of α-acids [11]. Additionally, the extraction of α-acids from the hops due to matrix effects, incomplete isomerization during the boil, adsorption of both α-acids and iso-α-acids on the trub are also greatly affected by the protonation state of α- and iso-α-acids [15].

Due to structural differences, many β-acids properties differ from those of α-acids. As β-acids do not contain a tertiary alcohol group in their aromatic nucleus, in contrast to hop α-acids they cannot isomerize [16]. The presence of another isoprenyl side chain causes the molecules to possess a more hydrophobic character. Therefore, compared to α-acids, β-acids are much less soluble in water. On the other hand, their unique structure is a source of antimicrobial properties [17], the ability to act against various microorganisms [18] and other physiological effects on the organisms of mammals [19]. β-acids in hops include a mixture of analogues with colupulone, lupulone and adlupulone being the most important ones. The content of other analogues, such as prelupulone and postlupolune, is minimal [20]. The most important property of beta acids that determines their behaviour during hop processing, storage and beer production, is their significant instability in the presence of oxygen and their susceptibility to oxidation reactions [12]. The antimicrobial activity of β-acids [17] is attributed to a range of congeners/analogues that have the alicyclic structure of 2,4-cyclohexadien-1-one. The most important structural features for their antibacterial properties include three non-polar isoprenyl chains that yield the whole molecule of β-acid a strongly hydrophobic character [21].

As described above, *Humulus lupulus* is a plant of great technological importance. Moreover, in a significant part of its applications, the α-acids and, to a lesser extent, β-acids play an important role. Fully protonated α- and β-acids are poorly soluble in water, while their solubility greatly increases with the increasing degree of deprotonation [22]. Additionally, the deprotonation of α-acids represents the first step in the isomerization of α-acids into iso-α-acids [11]. Consequently, the information on pK_a is of utmost importance for the understanding of *e.g.* the effect of pH during the worth boiling on the taste of the beer [15]. Moreover, the protonation state of α- and β-acids also affects their pharmacokinetics and their antibacterial activity [23]. Thus it is no surprise, that the pK_a values of α- and β-acids have already been determined [22–24]. The pK_a values reported for cohumulone and colupulone are 4.7 and 6.1, respectively [22–24]. Although α- and β-acids represent diprotic acids, only the first pK_a value is reported in the literature. Additionally, difficulties in determining these values are often reported due to relatively poor solubility in water. In the case of colupulone, even slightly different values can be found in the scientific literature (*e.g.* 5.93, reported by Schindler et al.) [25]. Furthermore, the reported constants are often determined in solutions with a relatively high share of MeOH [24], or a relatively high uncertainty was ascribed to reported values. If one compares the reported pK_a value of these compounds to values of other polyphenols [26], it may be seen, that the values are relatively low. One of the common explanations for the relatively low first pK_a value of α- and β-acids lies in their tautomerism [24,27]. Therefore, the goal of this study was also to determine which tautomer can provide a better explanation for the obtained spectroscopic data and, thereby yield a better insight into the deprotonation process of α- and β-acids on a molecular level. In the scientific literature, there is also still some disagreement regarding the cohumulones' stereochemistry [11,19,28,29]. This aspect will be addressed as well by combining CD-spectroscopy and TD-DFT calculations. All in all, this study should provide a better insight into the structure and pH-dependent behaviour of cohumulone and colupulone, which is crucial for their application in various beers as well as for their successful antimicrobial and cosmetic use.

2. Material and methods

2.1. High-performance liquid Chromatography (HPLC)

Analyses were performed on Vanquish Core analytical HPLC chromatograph (Thermoscientific, Waltham, USA) equipped with a PDA detector. The separations were carried on Eclipse XDB-C18 chromatographic column (Agilent Technologies, Santa Carla, USA, 5 μm) while (A) 0.1% formic acid aqueous solution (Carlo Erba reagents, Val-de-Reuil, France, v/v) in type I water (σ = 0.055 μS cm^{-1}) and (B) 0.1% formic acid (v/v) in acetonitrile (Honeywell Riedel de Haën, Seelze, Germany) were used as mobile phase. The chromatograms were monitored at various wavelengths, namely 280 nm (impurities), 330 nm (α-acids), and 370 nm (xanthohumol) (additionally UV–Vis spectra between 200 and 800 nm were collected). The mobile phase flow rate was set to 1 mL min^{-1}. Gradient: 0.0–3.0 min, 20.0–50.0% B; 3.0–6.0 min, 50.0–70.0% B; 6.0–15.0 min, 70.0–100.0% B; 15.0–21.8 min, 100.0% B; 21.8–22.0 min, 100.0–20.0% B; 22.0–27.0 min, 20.0% B.

2.2. Isolation and characterization of cohumulone and colupulone

2.2.1. Extraction

Dried hop cones were powdered and extracted using ultrasonic extraction with diethyl ether. 50 g of dried hop powder were mixed with 400 mL of diethyl ether and sonicated for 30 min at 25 °C. The supernatant was filtered and collected. Diethyl ether was evaporated using a rotary evaporator (Büchi, Flawil, Switzerland). The procedure was repeated 5 times and 20 g of hops extract was finally obtained.

2.2.2. Purification

Isolation was performed in three consecutive separations on C18 stationary phase. All separations were done using preparative chromatograph PuriFlash 5.250 (Interchim, Montluçon, France), equipped with PDA and ELSD detector. The desired amount of sample was dissolved in acetonitrile, filtered through 0.22 μm PTFE syringe filter and applied on the column. In all cases, chromatograms were observed at wavelengths of 280, 330, and 370 nm. Additionally, the dependence of UV/Vis spectra on retention time was followed. After each isolation step, the fractions were analysed for the content of compounds of interest using the method described in the HPLC Section 2.1. Fractions with desired purity were collected, and solvents evaporated using a rotary evaporator (Büchi, Flawil, Switzerland).

The first separation step was performed on the flash C18 PF-50C18HP-F0040 column (Interchim, Montluçon, France, 50 μm) using two solvents: (A) type (I) water with 0.1% formic acid, (B) acetonitrile with 0.1% formic acid. The following gradient with a flow rate of 26 mL/min was used: 0.0–2.0 min, 10.0% B; 2.0–27.0, 10.0–100.0% B. Finally, the column was washed with isopropanol and reconditioned for the subsequent separation.

The following two steps consisted of the semi-preparative separation on US10C18HQ-250/212 column (Interchim, Montluçon, France, 10 μm). The same mobile phases were applied as in the case of separations with flash chromatography ((A) type (I) water with 0.1% formic acid, (B) acetonitrile with 0.1% formic acid). Isocratic separation with 70% of mobile phase B (flow rate of 16 mL/min) was used to purify cohumulone. For purification of colupulone the following gradient was applied: 0.0–15.0 min, 70.0–100.0% B; 15.0–29.0 min, 100% B; reconditioning of column.

Finally, 380 mg of cohumulone and 411 mg of colupulone were obtained, and their chromatographic purity was determined using HPLC chromatography, as described in the HPLC section. A combination of a comparison of the HPLC retention time to the retention time of the standard and of the ^{1}H NMR spectrum to the literature values were used to confirm the structure of the two compounds.

2.3. Measurement of the UV/Vis spectra

All measurements were performed on Carry 4000 UV–Vis spectrophotometer equipped with a multiple cuvette thermostated holder (Agilent, USA) at a temperature of 298.15 K in the spectral range of 800–200 nm. The measurement step was 1 nm, and the averaging time for each step was 0.2 s. The Metrohm 780 pH-meter (Metrohm AG, Switzerland) equipped with Biotrode combined electrode (Metrohm AG, Switzerland) was applied to monitor the pH of prepared solutions. The buffer solutions employed were: (a) HCl (Honeywell, USA) and KCl (Supelco, Germany), pH 2.0–3.0; (b) NaOH (Sigma-Aldrich, Germany) and KCl (Supelco, Germany), pH 12.0; (c) Na_2HPO_4 and NaH_2PO_4 (Sigma-Aldrich, Germany), covering the pH range between 4.00 to 11.0, every 0.20±0.01 pH units. All buffer solutions were prepared with the same ionic strength (0.1 M). The compounds used to mix these solutions were of analytical reagent grade.

Cohumulone was dissolved in methanol (J. T. Baker, Poland) to prepare a stock solution with concentration of $6.63 \cdot 10^{-3}$ mol/L. For the UV/Vis measurements, a sufficient quantity of cohumulone stock solution was added to achive cohumulone concentration of $5.31 \cdot 10^{-5}$ mol/L with desired pH values between 2 and 12.2. Colupulone solutions were prepared using identical buffers, while Tween 80 (Sigma-Aldrich, Germany) solution was also added (final concentration of Tween 80 was 1%) to provide sufficient solubility of colupulone. Colupolone was dissolved in methanol to prepare a stock solution with concentration of $8.17 \cdot 10^{-3}$ mol/L. For the UV/Vis measurements, a sufficient quantity of colupolone stock solution was added to achieve colupolone concentration of $4.58 \cdot 10^{-5}$ mol/L with desired pH values between 2 and 12.2.

2.3.1. Determination of pK_a

For the determination of pK_a values the absorbances at wavelengths, where the most intensive changes in UV/Vis spectrum can be observed, were extracted from the pH dependence of UV/Vis spectrum. A model function (Eq. (1)) was fitted to experimental data using the least square method:

$$A = \frac{c \cdot l}{K_a + [H^+]}(\epsilon_{HA,\lambda} \cdot [H_3O^+] + \epsilon_{A,\lambda} \cdot K_a) \quad (1)$$

Where A, c, l, K_a, $\epsilon_{HA,\lambda}$, $\epsilon_{A,\lambda}$, and $[H_3O^+]$ represent model absorbance of sample, the analytical concentration of cohumulone/colupulone, cuvette optical path, acid dissociation constant, molar extinction coefficient of protonated and deprotonated species, and equilibrium concentration of H_3O^+ ions, respectively.

2.4. CD spectra

CD spectra were obtained on a JASCO J-1500 (Jasco, USA) automatic recording spectropolarimeter in a spectral range of 500–190 nm. The measurement step was 1 nm and the scanning speed was 100 nm/min. The instrument was calibrated with the recommended standard. Scan rates, sensitivities and repeat functions were selected to yield an optimal signal-to-noise ratio. Cohumulone was dissolved in methanol to prepare a stock solution of $6.63 \cdot 10^{-3}$ mol/L. For the CD measurements, a sufficient quantity of cohumulone stock solution was added to achieve cohumulone concentration of $3.32 \cdot 10^{-5}$ mol/L with desired pH values 2, 8.6 and 12.2.

2.5. Computational methods

Calculations were performed using the Gaussian 16 software package [30]. Geometry optimization of all possible cohumulone structures was done at the B3LYP level of theory [31–34] in conjunction with the flexible 6-311++G(d,p) basis set [35] in the implicit CPCM water model (ϵ = 78.3553). The obtained structures were examined using vibrational analysis in order to confirm that they represent true equilibrium geometries. The obtained structures were subsequently subjected to time-dependent density functional theory (TD-DFT) calculations to estimate the excited singlet-state properties using identical level of theory (B3LY/6-311++G(d,p)) and solvation model (CPCM). In each case, enough transitions were considered to reach a wavelength of 200 nm. Resulting absorption band wavelengths (λ_{max}) and oscillator strengths (f) were calculated for all allowed $\pi \rightarrow \pi^*$ and $n \rightarrow \pi^*$ transitions. Spectra were visualized following the procedure described in the Gaussian manual. The band broadening values (σ) of 0.3 eV and 0.50 eV were used for UV/Vis and CD spectra visualization, respectively, because these values provided the best reproduction of the experimental results. Avogadro 1.97.0 was applied for the visualization of Kohn–Sham orbitals [36].

3. Results and discussion

3.1. Isolation and characterization of cohumulone and colupulone

380 mg and 411 mg of cohumulone and colupulone were isolated by reverse phase preparative chromatography. The concentration of important hop constituents is typically determined at the wavelengths of 370 nm (xanthohumol), and 314 or 333 nm (α- or β-acids) [37,38]. These wavelengths are especially useful for the determination of concentration in complex samples with as little interference as possible. However, the purity of the sample can be overestimated if the purity of isolated compounds is examined at these wavelengths. To avoid that, the chromatographic purity was determined at a wavelength of 280 nm (Fig. 1) to be 98% and 93%, for cohumulone and colupulone, respectively. The identity of isolated compounds was confirmed by the comparison of their retention times to the retention times of cohumuolone and colupulone in ICE4 standard (NATECO2, Wolnzach, Mainburg, Germany) and by ^{1}H NMR spectroscopy [39,40].

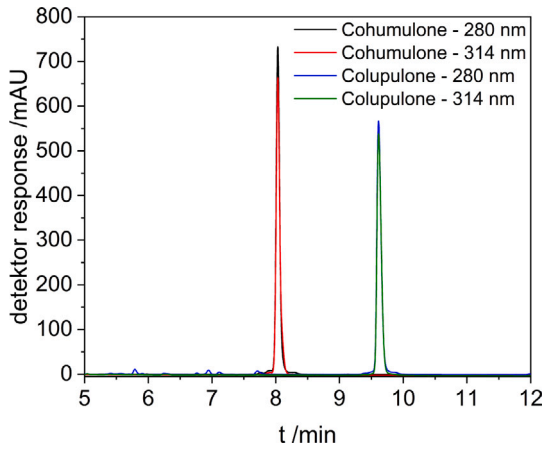

Fig. 1. Chromatographs of cohumulone and colupulone obtained at wavelengths of 280 nm and 314 nm.

3.2. pH dependence of spectra

Fig. 2 shows the dependence of the spectra of cohumulone and colupulone in aqueous solutions at different pH values. Due to the poor solubility of colupulone, the spectra were measured in the aqueous solution of 1% Tween 80 surfactant.

The formation of the insoluble precipitate can also be observed in the spectrum of cohumulone (Fig. 2(a)) at low pH values (below pH = 4.0) where the absorbance above $\lambda \approx 400$ nm is a consequence of poor solubility. A relatively broad peak can be seen in the wavelength range between 300 and 400 nm. When the wavelengths further decrease, the absorbance roughly increases, with two small peaks at wavelengths of approximately 280 and 240 nm. When the pH increases above the value of 4.0, a proper solution is formed, and, consequently, the absorbance above $\lambda = 400$ nm disappears. Additionally, the absorbance between 300 and 400 nm increases significantly, and two coalescent peaks at $\lambda = 364$ nm and $\lambda = 327$ nm are formed. With the increasing pH values, the intensity of these two peaks increases further up to pH = 6.0. Afterwards, their intensity remains relatively stable up to the pH value of 10.0, and decreases again above this pH value.

In the wavelength range between $\lambda = 200$ nm and $\lambda = 300$ nm, the peak at $\lambda \approx 276$ nm disappears with increasing pH values, while it reapers when the pH is increased above pH = 10.4. This newly formed peak is slightly blue-shifted compared to the peak at the lowest pH values (262 nm compared to the initial 276 nm), and its intensity increases up to a pH value of 12.2. A similar observation can be made for a peak at approximately 240 nm. It is firstly blue-shifted to the wavelength of 222 nm while its intensity increases with rising pH values. Moreover, the peak coalesces with an intensive peak, likely spreading to wavelengths below 200 nm.

The spectrum of colupulone at low pH values is similar to the spectrum of cohumulone. This is not surprising if one considers that the chromophores of both compounds are similar. At the lowest pH values, the wide peak at 330 nm with a shoulder at a wavelength of approximately 350 nm can be observed. The next peaks can be seen at wavelengths of 270 and 208 nm. However, the values below 205 nm may be unreliable due to the absorbance of the surfactant. When the pH increases, the intensity of the wide peak between 300 and 400 nm also rises. Moreover, the increase in peak intensity at $\lambda = 330$ nm with increasing pH values is less pronounced than the increase in peak intensity at $\lambda = 350$ nm. Consequently, the shape of the peak changes with the increasing pH — the absorption maximum of the peak at pH values higher than 6.0 is at 357 nm, and its shoulder is at a wavelength of approximately 330 nm. The change is taking place at higher pH values in the case of colupulone compared to cohumulone, which is a consequence of the higher pK_a value of colupulone [22–24]. The peak intensity at wavelength of 270 nm decreases with the increasing pH, and the absorption minimum is formed at $\lambda \approx 280$ nm when the pH reaches the value of 7.0. At pH values above 11.6, a new peak appears at the wavelength of 255 nm. Finally, the intensity of the peak with $\lambda = 208$ nm is increasing and redshifting with the rising pH.

From the pH-dependence of absorption, two pK_a values of cohumulone can be determined by fitting the experimental data to equation 1, which are 4.61 ± 0.15 and 11.6 ± 0.4 for the first and the second deprotonation of cohumulone, respectively. The first pK_a value is in a good agreement with the existing scientific literature (4.7) [23,24], while the second pK_a value was determined here for the first time. Similarly, the pK_a value of colupulone was obtained. Here, only the first pK_a value was determined, while the second deprotonation only begins at the higher border of the examined pH range. The first pK_a value is 6.06 ± 0.35, again in a good agreement with the existing scientific literature (6.1) [22]. However, one must keep in mind that the determination of this pK_a value is burdened with a high experimental uncertainty due to a relatively poor solubility of colupulone in aqueous media.

3.3. The species — comparison of experimental and calculated spectra

One of the goals of the present study was to determine which ionized species are most likely present in the cohumulone and colupulone aqueous solutions. There are two main reasons why this would be interesting. Firstly, cohumulone has two possible deprotonation positions, and understanding which deprotonation is taking place at a lower pH can influence our understanding of the reactivity of α–acids. The second reason is that the relatively low pK_a value of cohumulone is traditionally ascribed to its possible tautomerism [24]. The aim of this study was also to determine to what degree the tautomer contributes to the shape of the spectrum.

To obtain this information, the UV/Vis spectra of all possible species of cohumulone and colupulone (Fig. 3) were calculated and compared to experimental UV/Vis spectra [41]. Because each cohumulone molecule has three side chains, the effect of the rotation of these chains on UV/Vis spectra and especially CD spectra was also examined. UV/Vis spectra of all rotamers are depicted in the Figure S1 of Supplementary Material, while only the best representatives of each species are depicted in the main article (Fig. 5).

Calculations were initiated by examining the influence of rotation of side chains of cohumulone. In all cases, the rotation of the carbonyl group was examined first. For these rotamers, a single energetically favoured position was found — consequently, only that position was considered for subsequent spectra calculations. Reason for a single energetically favoured position can be sought in the formation of intramolecular hydrogen bonds (C0, Ct0, C1b, Ct1b) and steric hindrances (C1a and C2). Three favourable positions were allocated when the alkyl chain on the chiral C-atom was rotated (see Figs. 4(a) and 4(c)). Additionally, two favourable rotamers were found when the third alkyl chain was rotated (see Fig. 4(a)–4(d)). The structures presented in Fig. 4 form the most abundant conformers of cohumulone neutral species C0.

From Figure S1 of Supplementary Material, one can see that the position of side chains of cohumulone indeed affects the peak positions and absorption coefficients of the calculated spectrum. However, the effect is not too significant since it only slightly varies the positions of absorption bands while the changes in the intensity of absorption lines are a bit more pronounced. In Fig. 5(a), the comparison of experimental (pH = 2.00) and calculated spectra for one of the rotamers of C0 and Ct0 is depicted. While plotting other rotamers will give us slightly different numbers, the spectra would be qualitatively the same (see Figure S1a–b).

At pH = 2.0 only the neutral species of cohumulone is expected (more than 99 % molar share). The comparison of experimental and

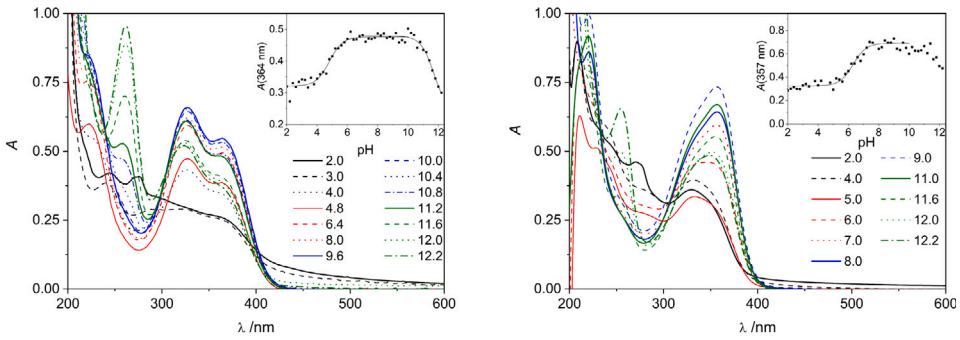

(a) (b)

Fig. 2. pH dependance of experimental spectra of cohumulone (2(a); $c = 5.31 \cdot 10^{-5}$ mol/L) and colupulone (2(b); $c = 4.58 \cdot 10^{-5}$ mol/L).

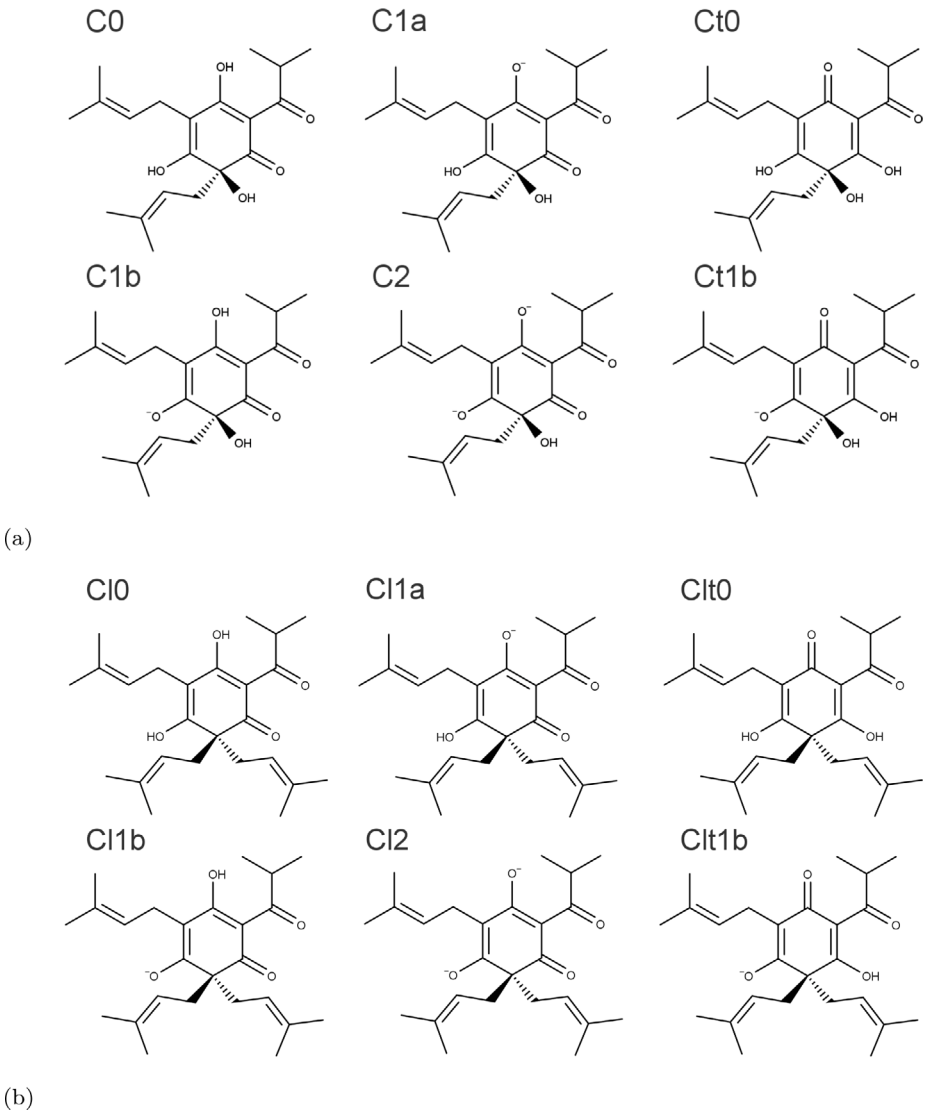

(a)

(b)

Fig. 3. Structures of cohumulone (3(a)) and colupulone (3(b)) taken into consideration in the calculation of the UV/Vis spectrum of cohumulone and colupolone [28].

calculated spectrum is depicted in Fig. 5(a). One can see that this spectrum differs from the spectrum for pH = 2.0 shown in Fig. 2(a). This is because the spectrum in Fig. 2(a) is affected by the precipitation of cohumulone. Consequently, we measured an additional spectrum with the addition of Tween 80 surfactant. However, the spectrum obtained for cohumulone in water at a pH value of 3.0 closely resembles the spectrum of cohumulone in water with the addition of surfactant at pH = 2.0. So, it can be concluded that the presence of surfactant does not significantly alter the UV/Vis spectrum of cohumulone. One can observe that species C0 reproduces the experimental spectrum at pH = 2.0 much better than its tautomer Ct0. Moreover, the Gibbs free energy of species C0 is 5.8 kcal/mol lower than the free energy of

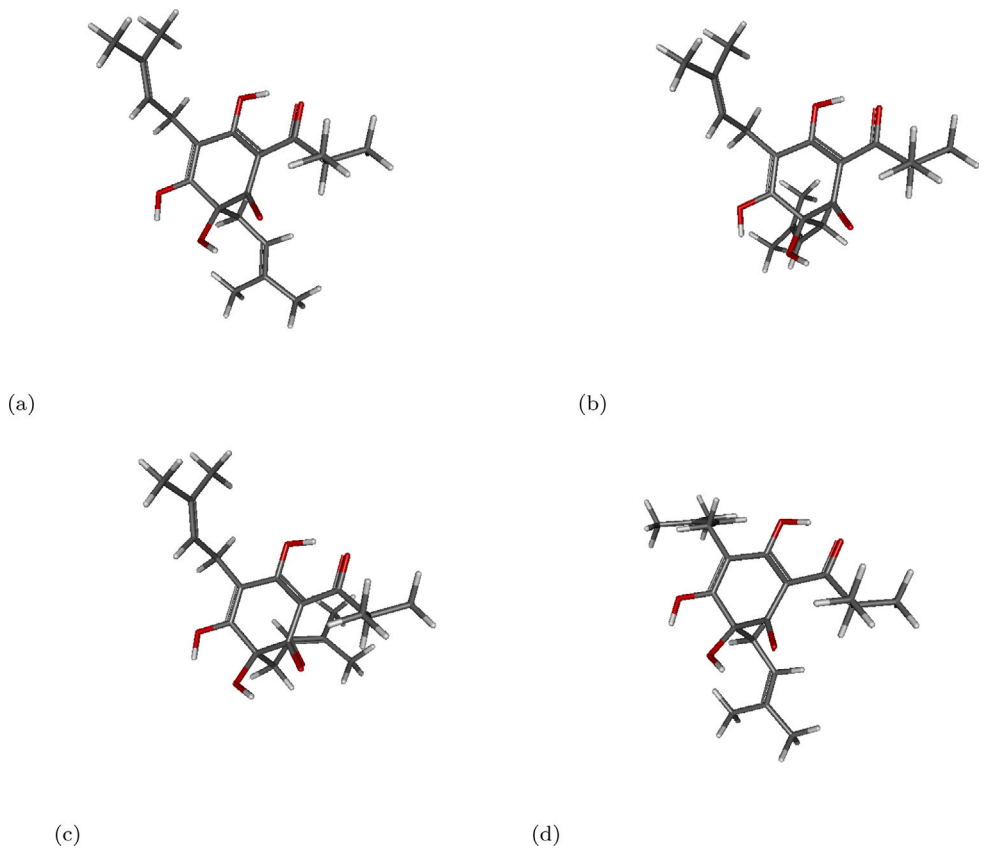

Fig. 4. 3D structures applied for calculations of spectra of neutral (C0) species.

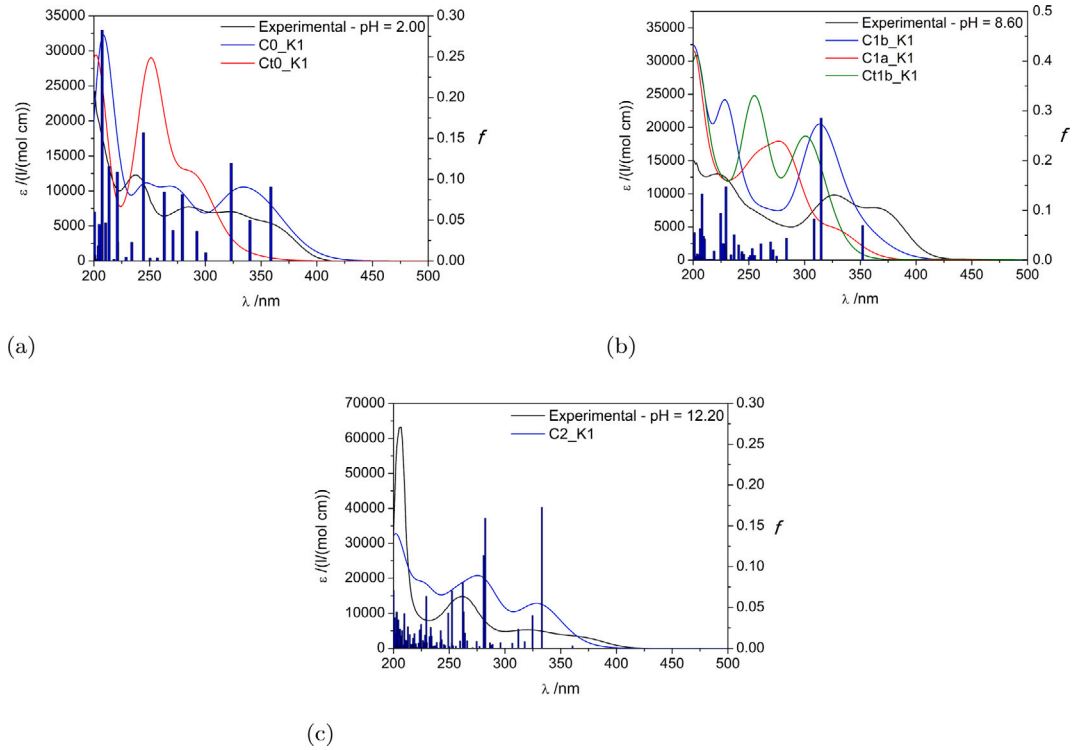

Fig. 5. Comparison of experimental and calculated UV/Vis spectra for different species of cohumulone. Additionally, oscillator strengths (f) of species most likely present in the aqueous solution are depicted as blue columns.

species Ct0. Moreover, three main peaks with several shoulders are present in the experimental spectrum. Namely, peak at $\lambda = 200$ nm with a shoulder at $\lambda \approx 206$ nm, peak with a maximum at $\lambda = 238$ nm and finally, a wide peak in the range between wavelengths of $\lambda = 260$ nm

and $\lambda = 420$ nm, consisting from two convoluted peaks with maximum absorption at wavelengths of 285 nm and 323 nm, as well as a shoulder at a wavelength of $\lambda \approx 360$ nm. The shoulder at $\lambda \approx 364$ nm, is most likely a consequence of the HOMO→LUMO transition, resulting in a calculated absorption band at $\lambda = 358.77$ nm (see Fig. 6 for the depiction of orbital shapes, and Table S1 of Supplementary Material for list of transitions). At the same time, HOMO-1→LUMO ($\lambda = 339.97$ nm) and HOMO-2→LUMO ($\lambda = 323.19$ nm) transitions correspond to the peak in the experimental spectrum at a wavelength of 323 nm. The peak at the wavelength of 285 nm is a consequence of 5 transitions, with HOMO→LUMO+1 ($\lambda = 279.38$ nm) and HOMO-2→LUMO+1 ($\lambda = 263.21$ nm) being the most pronounced. The transitions HOMO-5→LUMO ($\lambda = 244.49$ nm) and HOMO-6→LUMO ($\lambda = 234.03$ nm) further correspond to the experimental peak at $\lambda = 238$ nm. Finally, the peak with the shoulder at $\lambda \approx 206$ nm results from several absorption bands with HOMO→LUMO+5 transition exhibiting the highest intensity.

At pH = 8.6, cohumulone is, according to the determined pK_a values, virtually exclusively (99.9%) present as once deprotonated species. Compared to the experimental spectrum at pH = 2.0, the intensity of peaks below the wavelength of 308 nm is decreased while the intensity of the two peaks above this wavelength increases. The second feature is well explained by the calculated spectrum of C1b (see Fig. 5(b)). If the calculated spectra of species C1a and Ct1b are compared to the experimental spectrum and to the spectrum of species of C1b, one can see that the spectra of C1a and Ct1b are strongly blue-shifted. Moreover, the species C1b also exhibits the lowest Gibbs free energy, 11.1 and 8.9 kcal/mol, lower than the free energy of species C1a and Ct1b, respectively. Furthermore, although the two peaks in the wavelength range between 300 nm and 400 nm are not the best reproduced in the calculated spectrum of C1b, one should remember that calculated spectra are visualized with arbitrary peak broadening values. The application of smaller peak broadening values would indeed result in two peaks since three main absorption lines are present in the area, one being significantly separated from the other two (see Fig. 5(b)). According to TD-DFT calculations, the experimental peak at $\lambda = 364$ nm is a consequence of HOMO→LUMO transition ($\lambda = 352.01$ nm), while the experimental peak at $\lambda = 327$ nm is a consequence of HOMO→LUMO+1 ($\lambda = 314.90$ nm) and HOMO-1→LUMO ($\lambda = 308.53$ nm) transitions. In the experimental spectrum, an additional peak can be observed at $\lambda = 222$ nm, which the HOMO-5→LUMO ($\lambda = 229.45$ nm) absorption band can explain. The last peak in the experimental spectrum at $\lambda = 201$ nm is, according to TD-DFT calculations, a consequence of multiple transitions.

Finally, at pH 12.2, cohumulone is present primarily as a twice deprotonated (80%) compound. Although there is also some share of once-deprotonated cohumulone, the experimental spectrum at this pH value was considered for comparison with the calculated spectrum of the C2 species since it is the spectrum with the highest pH value available. Comparing the experimental spectrum to the spectrum at pH = 8.6, one can see that absorbance at wavelengths above 293 nm is decreased, while a new peak arose at $\lambda = 262$ nm and the peak at $\lambda = 221$ nm disappears. Additionally, the intensity of the peak at the $\lambda = 207$ nm is strongly enhanced. If the calculated spectra of C1b and C2 are compared, one may see that these changes (decreased absorbance at high wavelengths, appearance of a new peak at $\lambda = 221$ nm) are well reproduced. According to TD-DFT calculations, the shoulder in the experimental spectrum at $\lambda \approx 364$ nm is a consequence of HOMO→LUMO transition at the wavelength of 360.57 nm, while the experimental peak at $\lambda = 320$ nm is a consequence of HOMO→LUMO+1 transition at $\lambda = 333.13$ nm. Moreover, the peak at $\lambda = 262$ nm is, according to TD-DFT calculations, a consequence of several transitions, a HOMO-2→LUMO transition ($\lambda = 282.31$ nm) being the most pronounced.

An analogous comparison with experimental spectra was performed also for the calculated UV/Vis spectra of colupulone species. Here, the analysis of rotamers was omitted because colupulone does not represent a chiral molecule and, therefore, is not CD-active. Moreover, in the case of cohumulone it was demonstrated that different rotamers do not significantly affect the shape of the UV/Vis spectrum. The orbitals taking place in the transitions are depicted in Fig. 8, while the list of electronic transitions is provided in Table S2 of Supplementary Material. In Fig. 7(a), the comparison of calculated spectra of both neutral species (Cl0 and Clt0) with the experimental spectrum is presented. One can see that the agreement between calculated and experimental results is much better for Cl0 species, indicating that this species is most likely prevalent at low pH values. The relatively wide peak in the region between wavelengths of 310 and 400 nm can be explained by HOMO→LUMO ($\lambda = 345.04$ nm) and HOMO-3→LUMO ($\lambda = 312.93$ nm) transitions. The next peak at a wavelength of approximately 284 nm is a consequence of two main absorption bands, namely HOMO→LUMO+1 and HOMO-1→LUMO+1 with wavelengths of 277.61 and 270.19 nm, respectively. The absorption around and below 250 nm can be largely ascribed to HOMO-6→LUMO transition at $\lambda = 238.84$ nm. Finally, the peak at the wavelength of 212 nm in experimental spectrum is a consequence of many transitions, where HOMO→LUMO+7 ($\lambda = 209.89$ nm) absorption band is the most important.

At higher pH values, where the once-deprotonated species is prevalent, the experimental spectrum is compared to the spectra of three species, namely Cl1a, Cl1b, and Ct1b. Here, the agreement of the UV/Vis spectrum of two species, Cl1a and Cl1b, with the experimental spectrum is good. However, since the Gibbs free energy of species Cl1b is 14.3 kcal/mol lower than the free energy of species Cl1a, it can be assumed that the Cl1b is prevalent in the solution. The peak at 357 nm and the shoulder at the wavelength of approximately 330 nm are consequences of HOMO→LUMO and HOMO→LUMO+1 transitions with $\lambda =$ nm and $\lambda =$ nm, respectively. Moreover, the shoulder in experimental spectrum at the wavelength of 220 nm is a consequence of HOMO-6→LUMO+1 ($\lambda = 224.43$ nm) absorption band. To explain the absorption in experimental spectra at wavelengths of 240–300 nm and below 212 nm, several absorption bands of relatively low intensity need to be considered.

Finally, the experimental spectrum at the highest pH value is compared to the calculated UV/Vis spectrum of twice-deprotonated species Cl2. It can be seen that the agreement between both spectra is very good. The broad peak in the experimental spectrum at the wavelength of 348 nm can be explained by two electronic transitions, HOMO→LUMO and HOMO→LUMO+3, with wavelengths of 335.01 and 334.70 nm, respectively. According to the results of TD-DFT calculations, two additional peaks in the experimental spectrum at wavelengths of 255 and 208 nm result from multiple electronic transitions.

Comparing the calculated and experimental spectrum can help us determine the exact species most likely present in the aqueous solution. Following this procedure, we can say that the neutral species present in the cohumulone solution is C0, once-deprotonated species is C1b, and the twice-deprotonated species is C2. In the case of colupulone, the species most likely present in solutions of low, intermediate and high pH are Cl0, Cl1b, and Cl2, respectively, indicating that tautomeric species Clt0 and Clt1b are not present in the solution or are present in minor molar fractions only. Furthermore, the species whose calculated UV/Vis spectra are the most similar to the experimental spectra are also thermodynamically favoured. So it can be concluded that the first deprotonation position is the same for cohumulone and colupulone (see structures C1b and Cl1b in Fig. 3), while tautomerism does not play an important role in the deprotonation process.

3.3.1. Calculated and experimental CD spectrum

Cohumulone represents, as all α-acids, a chiral compound. Stereoisomery of α-acids does not affect the stereochemistry of iso-α-acids, but knowing the right configuration at the chiral centre is likely important for the understanding of the antibacterial and other health-enhancing properties of α-acids. Although the spatial configuration of cohumulone atoms has already been determined using X-ray diffraction [28], a

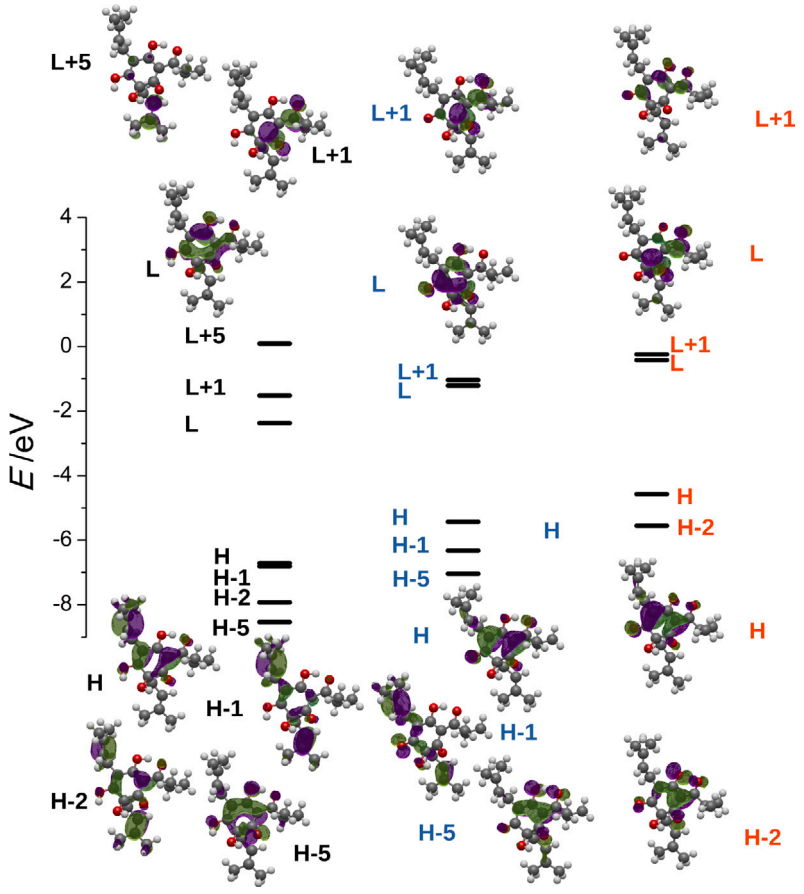

Fig. 6. Depiction of main orbitals taking place in the most important electronic transitions of cohumulone that result in its UV/Vis spectrum. The black, blue and orange orbital denotations represents the C0, C1b, and C2 species, respectively.

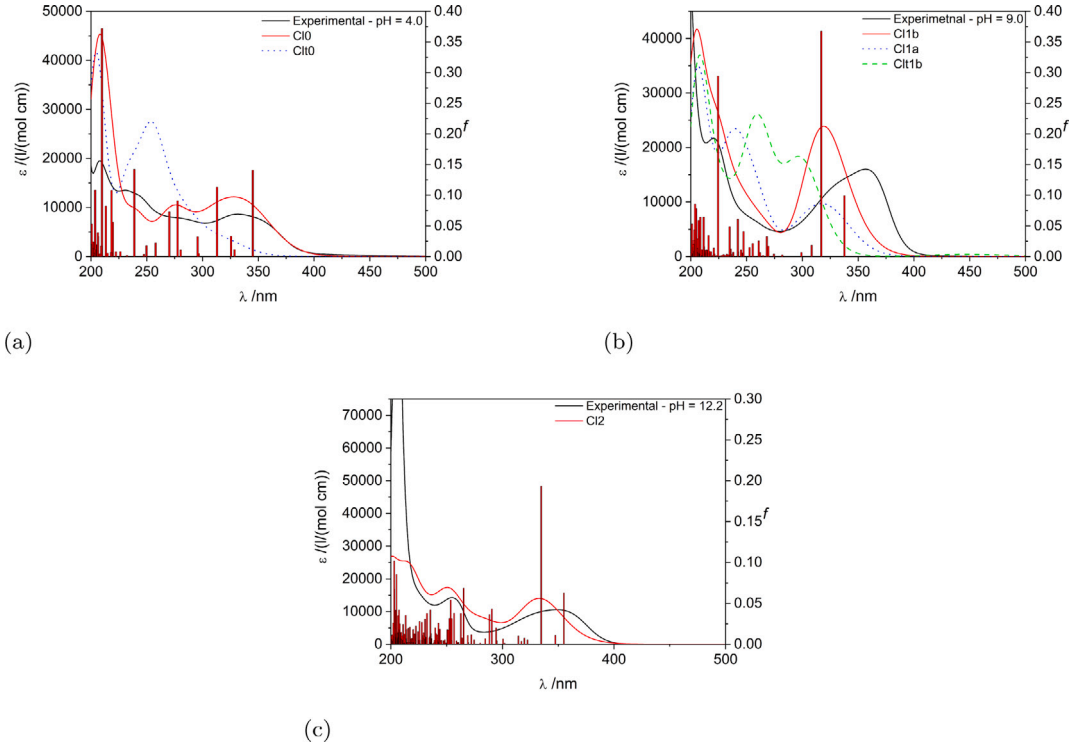

Fig. 7. Comparison of experimental and calculated UV/Vis spectra for different species of colupulone. Additionally, oscillator strengths (f) for species most likely present in the aqueous solution are depicted as red columns.

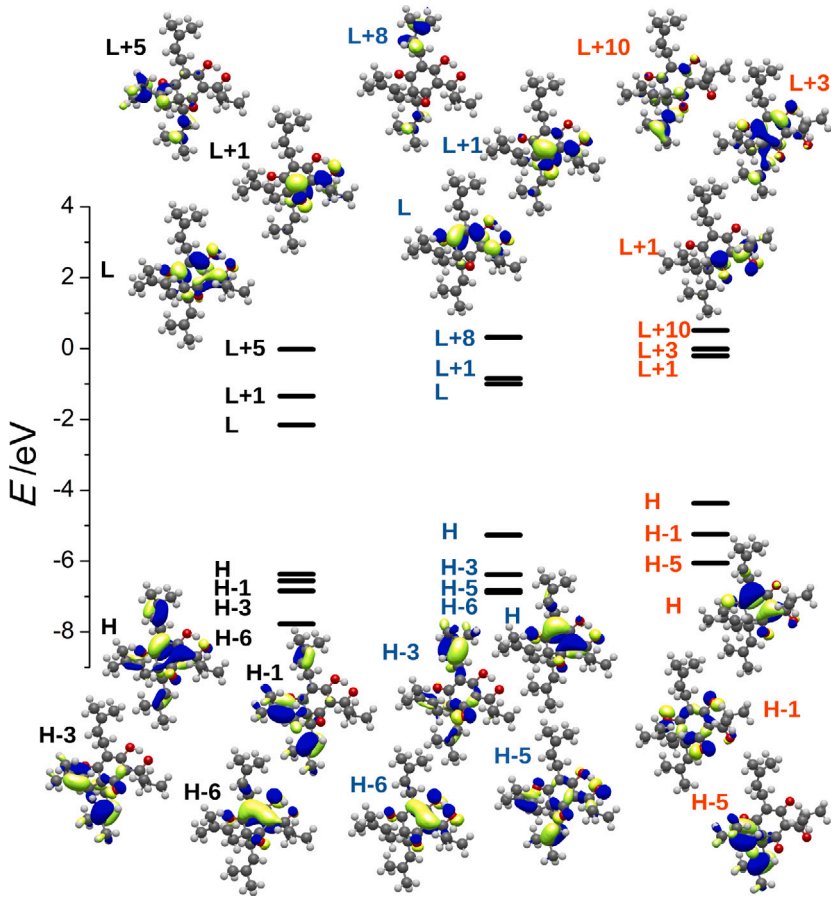

Fig. 8. Depiction of main orbitals taking place in the most important electronic transitions of colupulone that result in its UV/Vis spectrum, where the black, blue and orange orbital denotations represents the Cl0, Cl1b, and Cl2 species, respectively.

wrong stereo configuration can still be often found in the scientific literature [11,19,29].

One of the optical methods that can distinguish between compounds of different stereoconfiguration is CD-spectroscopy. So to confirm the validity of the cohumulone stereoconfiguration established by X-ray diffraction as well as to demonstrate how this relatively simple method with minimal need for sample preparation can be applied for the determination of the absolute configuration on a chiral centre. Therefore, the calculated CD spectra were compared to the experimental ones also for an additional validation of species present in the aqueous solutions.

CD spectra were calculated for all the optimized structures previously applied in the calculation of UV/Vis spectra. The spectra of all used rotamers are depicted in Figure S2 of Supplementary Material. It is possible to see that the influence of the 3D configuration of the side chains is way more pronounced here than in UV/Vis spectrometry, with different configurations even being able to change the sign of a peak in a certain wavelength section. For neutral species C0, the agreement between experimental and calculated data is excellent for wavelengths between 275 and 425 nm. The negative peak at a wavelength of ≈ 360 nm is correctly reproduced in the calculations of all species, while two peaks at ≈ 305 and ≈ 275 nm have their corresponding counterparts in the calculated spectrum. The agreement is slightly worse for the wavelengths between 250 and 275 nm, where the positive value in the experimental spectrum is correctly reproduced solely by one of the rotamers (C0_K1_A2). However, in the next spectral region, 220 to 260 nm, the agreement between experimental and calculated spectra is again rather good. The wide negative peak is reproduced by three negative rotatory strengths in that section. However, in the case of rotamer C0_K1, there are two slightly positive rotatory strengths and, consequently, a small peak in the visualized spectrum. But its size is, to a certain degree a consequence of an arbitrarily selected peak widening value and would disappear if this value was increased. At the lowest wavelengths, there is a positive signal in the experimental CD spectrum, which is well reproduced also in the calculated spectrum of C0.

In Fig. 9 the comparison of calculated CD spectra of various species with the experimental cohumulone spectra is depicted. One can see that the peak at ≈ 360 nm in the experimental spectrum is correctly reproduced by species C0 and Ct0. For the next spectral range (peaks at ≈ 305 and ≈ 275 nm) the agreement between the experimental spectrum and the spectrum of Ct0 is worse than between the experimental spectrum and the spectrum of C0. Finally, at the lowest wavelengths, the experimental spectrum is well reproduced by both examined species. In Fig. 9, an additional spectrum is depicted for the C0 species with the reversed (*R*) stereoisomery on the chiral carbon atom (species C0_N). It is easy to see that the sign of the signal for this species is just the opposite of the sign of the experimental spectrum. This confirms that the correct stereoconfiguration on the cohumulone chiral carbon atom is indeed *S* and not *R* [28].

3.4. Conclusions

To sum everything up, we performed UV/Vis titration of aqueous solutions of cohumulone and colupulone and obtained corresponding pK_a values that are in a good agreement with existing scientific literature data. Moreover, the second pK_a value of cohumulone (pK_a = 11.6) was determined here for the first time. The UV/Vis and CD spectra of cohumulone and UV/Vis spectra of colupulone were collected at pH values, were neutral, once-deprotonated and twice-deprotonated species should be prevalent. These experimental spectra were compared to the calculated spectra of all possible species of cohumulone and

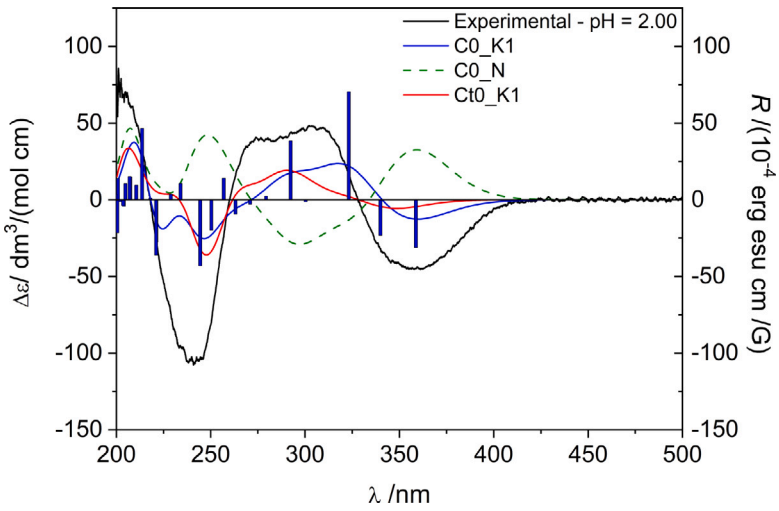

Fig. 9. Comparison of experimental and calculated CD spectra of neutral species of cohumulone. Additionally, a CD spectrum of neutral species with the wrong (*R*) stereochemistry on the chiral carbon atom (C0_N) is depicted. Finally, rotatory strengths R for species most likely present in the aqueous solution are presented as blue columns.

colupulone. The species most likely present in the aqueous solution at a certain pH were determined based on the best agreement between the calculated and experimental spectra. These neutral, once-deprotonated and twice-deprotonated species are C0, C1b and C2 in the case of cohumulone and Cl0, Cl1b and Cl2 in the case of colupulone, respectively. Last but not least, from the CD spectrum of cohumulone at a low pH value, its absolute stereoconfiguration was determined as the one depicted in Fig. 3 (with the *S* configuration on the chiral carbon atom).

Funding

This work was supported by the Slovenian Research and Innovation Agency (ARIS), Slovenia through programme and project grants J1-2471, P2-0046, L2-3175, J4-4633, J1-4398, L2-4430, J3-4498, J7-4638, J1-4414, J3-4497, P2-0438, and I0-E015.

CRediT authorship contribution statement

Anja Petek: Writing – original draft, Investigation, Formal analysis, Data curation, Conceptualization. **Urban Bren:** Writing – review & editing, Supervision, Resources, Project administration, Methodology, Funding acquisition. **Gregor Hostnik:** Writing – review & editing, Writing – original draft, Visualization, Supervision, Methodology, Investigation, Formal analysis, Conceptualization.

Declaration of competing interest

The authors declare that they have no known competing financial interests or personal relationships that could have appeared to influence the work reported in this paper.

Data availability

Data will be made available on request.

Acknowledgements

The help of Matej Keber in isolation of cohumulone and colupulone is gratefully acknowledged. The authors thank Dr. Matja Zalar for measurements of ^{1}H NMR spectra. The authors thank the Slovenian NMR centre at the National Institute of Chemistry for the opportunity to perform NMR experiments. The authors are grateful to Katarina Kores and Dr. Jelena Tošević for the discussion on TD-DFT calculations. Marvin 17.21.0, Chemaxon (https://www.chemaxon.com) was used for drawing and displaying chemical structures. The authors acknowledge the use of research equipment UV/Vis and CD spectrophotometer, procured within the project "Upgrading national research infrastructures - RIUM", which was co-financed by the Republic of Slovenia, the Ministry of Higher Education, Science and Innovation and the European Union from the European Regional Development Fund.

Appendix A. Supplementary data

Supplementary material related to this article can be found online at https://doi.org/10.1016/j.saa.2024.124593.

References

[1] D.P. Killeen, D.H. Andersen, R.A. Beatson, K.C. Gordon, N.B. Perry, Vibrational spectroscopy and chemometrics for rapid, quantitative analysis of bitter acids in hops (*Humuluslupulus*), J. Agric. Food Chem. 62 (52) (2014) 12521–12528, http://dx.doi.org/10.1021/jf5042728.

[2] T.R. Arruda, P.F. Pinheiro, P.I. Silva, P.C. Bernardes, A new perspective of a well-recognized raw material: Phenolic content, antioxidant and antimicrobial activities and α- and β-acids profile of Brazilian hop (*Humulus lupulus L.*) extracts, LWT 141 (2021) 110905, http://dx.doi.org/10.1016/j.lwt.2021.110905.

[3] P. Zanoli, M. Zavatti, Pharmacognostic and pharmacological profile of *Humulus lupulus L.*, J. Ethnopharmacol. 116 (3) (2008) 383–396, http://dx.doi.org/10.1016/j.jep.2008.01.011.

[4] P. Zanoli, M. Rivasi, M. Zavatti, F. Brusiani, M. Baraldi, New insight in the neuropharmacological activity of *Humulus lupulus L.*, J. Ethnopharmacol. 102 (1) (2005) 102–106, http://dx.doi.org/10.1016/j.jep.2005.05.040.

[5] K. Hong, Z. Xu, L. Wang, A. Johnpaul, Y. Cheng, C. Lv, C. Ma, Varietal differences in the phytochemical components' accumulation and aroma profile of three *Humulus lupulus* cultivars, Food Control 132 (2022) 108499, http://dx.doi.org/10.1016/j.foodcont.2021.108499.

[6] M. Knez Hrnčič, E. Španinger, I.J. Košir, Ž. Knez, U. Bren, Hop compounds: Extraction techniques, chemical analyses, antioxidative, antimicrobial, and anticarcinogenic effects, Nutrients 11 (2) (2019) 257, http://dx.doi.org/10.3390/nu11020257.

[7] K. Hong, L. Wang, A. Johmpaul, C. Lv, C. Ma, Key enzymes involved in the synthesis of hops phytochemical compounds: From structure, functions to applications, Int. J. Mol. Sci. 22 (17) (2021) 9373, http://dx.doi.org/10.3390/ijms22179373.

[8] L.C. Verhagen, 3.22 - Beer flavor, in: H.-W.B. Liu, L. Mander (Eds.), Comprehensive Natural Products II, Elsevier, Oxford, 2010, pp. 967–997, http://dx.doi.org/10.1016/B978-008045382-8.00087-3.

[9] M. Van Cleemput, K. Cattoor, K. De Bosscher, G. Haegeman, D. De Keukeleire, A. Heyerick, Hop (*Humulus lupulus*)-derived bitter acids as multipotent bioactive compounds, J. Nat. Prod. 72 (6) (2009) 1220–1230, http://dx.doi.org/10.1021/np800740m.

[10] A.J. Arduengo III, S.F. Gamper, J.C. Calabrese, F. Davidson, Low-coordinate carbene complexes of nickel(0) and platinum(0), J. Am. Chem. Soc. 116 (10) (1994) 4391–4394, http://dx.doi.org/10.1021/ja00089a029.

[11] B. Jaskula, P. Kafarski, G. Aerts, L. De Cooman, A kinetic study on the isomerization of hop α-acids, J. Agric. Food Chem. 56 (15) (2008) 6408–6415, http://dx.doi.org/10.1021/jf8004965.
[12] M. Verzele, Practical aspects of the isomerization of *alpha*-acids, in: Proc. Eur. Brew. Conv. Congr. Stockholm, 1965, pp. 398–404.
[13] H. Köller, Die katalytische beschleunigung der isomerisierung von humulon zu isohumulonen durch metallionen, Tetrahedron Lett. 9 (40) (1968) 4317–4320.
[14] D. Lance, A. White, R. Hildebrand, B. Clarke, The effect of heat on metal humulate and isohumulate salts, J. Inst. Brew. 81 (5) (1975) 364–367.
[15] B. Jaskula-Goiris, G. Aerts, L. De Cooman, Hop α-acids isomerisation and utilisation: an experimental review, Cerevisia 35 (3) (2010) 57–70, http://dx.doi.org/10.1016/j.cervis.2010.09.004.
[16] J. Li, N. Li, X. Li, G. Chen, C. Wang, B. Lin, Y. Hou, Characteristic α-acid derivatives from humulus lupulus with antineuroinflammatory activities, J. Nat. Prod. 80 (12) (2017) 3081–3092, http://dx.doi.org/10.1021/acs.jnatprod.6b00921.
[17] Z. Kolenc, T. Langerholc, G. Hostnik, M. Ocvirk, S. Štumpf, M. Pintarič, I.J. Košir, A. Čerenak, A. Garmut, U. Bren, Antimicrobial properties of different hop (*Humulus lupulus*) genotypes, Plants 12 (1) (2023) http://dx.doi.org/10.3390/plants12010120.
[18] M. Arczewska, D.M. Kamiński, B. Gieroba, M. Gagoś, Acid–base properties of xanthohumol: A computational and experimental investigation, J. Nat. Prod. 80 (12) (2017) 3194–3202, http://dx.doi.org/10.1021/acs.jnatprod.7b00530.
[19] M. Karabín, T. Hudcová, L. Jelínek, P. Dostálek, Biologically active compounds from hops and prospects for their use, Compr. Rev. Food Sci. Food Saf. 15 (3) (2016) 542–567, http://dx.doi.org/10.1111/1541-4337.12201.
[20] J.J.C. Scheffer, Chemistry and analysis of hop and beer bitter acids; developments in food science, Flavour Fragr. J. 8 (3) (1993) 169, http://dx.doi.org/10.1002/ffj.2730080308.
[21] Schmalreck, Structural features determining the antibiotic potencies of natural and synthetic hop bitter resins, their precursors and derivatives, Can. J. Microbiol. 21 (2) (1975) 205–212, http://dx.doi.org/10.1139/m75-029.
[22] W.J. Simpson, Ionization behaviour of hop compouns and hop-derived compounds, J. Inst. Brew. 99 (4) (1993) 317–326, http://dx.doi.org/10.1002/j.2050-0416.1993.tb01169.x.
[23] W. Simpson, A. Smith, Factors affecting antibacterial activity of hop compounds and their derivatives, J. Appl. Microbiol. 72 (4) (1992) 327–334, http://dx.doi.org/10.1111/j.1365-2672.1992.tb01843.x.
[24] S. R., The chemistry of hop constituents, in: D.E. Briggs, C.A. Boulton, P.A. Brookes, R. Stevens (Eds.), Brewing, in: Woodhead Publishing Series in Food Science, Technology and Nutrition, Woodhead Publishing, 2004, pp. 255–305, http://dx.doi.org/10.1533/9781855739062.255.
[25] R. Schindler, Z. Sharrett, M.J. Perri, M. Lares, Quantification of α-acids in fresh hops by reverse-phase high-performance liquid chromatography, ACS Omega 4 (2) (2019) 3565–3570, http://dx.doi.org/10.1021/acsomega.9b00016.
[26] J. Beltrán, N. Sanli, G. Fonrodona, D. Barrón, G. Özkan, J. Barbosa, Spectrophotometric, potentiometric and chromatographic pka values of polyphenolic acids in water and acetonitrile–water media, Anal. Chim. Acta 484 (2) (2003) 253–264, http://dx.doi.org/10.1016/S0003-2670(03)00334-9.
[27] M. Collins, D.R.J. Laws, J.D. McGuinness, J.A. Elvidge, Chemistry of hop constituents. Part xxxVIII. Alkenylation of 2-acylcyclohexane-1, 3, 5-triones and further evidence concerning the fine structure of hop β-acids, J. Chem. Soc. C (1971) 3814–3818, http://dx.doi.org/10.1039/J39710003814.
[28] J. Urban, C.J. Dahlberg, B.J. Carroll, W. Kaminsky, Absolute configuration of beer's bitter compounds, Angew. Chem. 52 (5) (2013) 1553–1555, http://dx.doi.org/10.1002/anie.201208450.
[29] S. Sun, X. Wang, A. Yuan, J. Liu, Z. Li, D. Xie, H. Zhang, W. Luo, H. Xu, J. Liu, C. Nie, H. Zhang, Chemical constituents and bioactivities of hops (*Humulus lupulus L.*) and their effects on beer-related microorganisms, Food Energy Secur. 11 (2) (2022) e367, http://dx.doi.org/10.1002/fes3.367.
[30] M.J. Frisch, G.W. Trucks, H.B. Schlegel, G.E. Scuseria, M.A. Robb, .G.S. J. R. Cheeseman and, V. Barone, G.A. Petersson, H. Nakatsuji, X. Li, M. Caricato, A.V. Marenich, J. Bloino, B.G. Janesko, R. Gomperts, B. Mennucci, H.P. Hratchian, J.V. Ortiz, A.F. Izmaylov, J.L. Sonnenberg, D. Williams-Young, F. Ding, F. Lipparini, F. Egidi, J. Goings, B. Peng, A. Petrone, T. Henderson, D. Ranasinghe, V.G. Zakrzewski, J. Gao, N. Rega, G. Zheng, W. Liang, M. Hada, M. Ehara, K. Toyota, R. Fukuda, J. Hasegawa, M. Ishida, T. Nakajima, Y. Honda, O. Kitao, H. Nakai, T. Vreven, K. Throssell, J.A. Montgomery, J.E. Peralta, F. Ogliaro, M.J. Bearpark, J.J. Heyd, E.N. Brothers, K.N. Kudin, V.N. Staroverov, T.A. Keith, R. Kobayashi, J. Normand, K. Raghavachari, A.P. Rendell, J.C. Burant, S.S. Iyengar, J. Tomasi, M. Cossi, J.M. Millam, M. Klene, C. Adamo, R. Cammi, J.W. Ochterski, R.L. Martin, K. Morokuma, O. Farkas, J.B. Foresman, D.J. Fox, Gaussian 16 Revision C.01, Gaussian Inc. Wallingford CT, 2016.
[31] A.D. Becke, DensityFunctional thermochemistry. III. the role of exact exchange, J. Chem. Phys. 98 (7) (1993) 5648–5652, http://dx.doi.org/10.1063/1.464913.
[32] C. Lee, W. Yang, R. Parr, Development of the colle-salvetti correlation-energy formula into a functional of the electron density, Phys. Rev. B 37 (2) (1988) 785–789, http://dx.doi.org/10.1103/PhysRevB.37.785.
[33] S.H. Vosko, L. Wilk, M. Nusair, Accurate spin-dependent electron liquid correlation energies for local spin density calculations: a critical analysis, Can. J. Phys. 58 (8) (1980) 1200–1211, http://dx.doi.org/10.1139/p80-159.
[34] P.J. Stephens, F.J. Devlin, C.F. Chabalowski, M.J. Frisch, Ab initio calculation of vibrational absorption and circular dichroism spectra using density functional force fields, J. Phys. Chem. 98 (45) (1994) 11623–11627, http://dx.doi.org/10.1021/j100096a001.
[35] W.J. Hehre, L. Radom, P. Schleyer, J.A. Pople, Ab Initio Molecular Orbital Theory, first ed., John Wiley, New York, 1986.
[36] M.D. Hanwell, D.E. Curtis, D.C. Lonie, T. Vandermeersch, E. Zurek, G.R. Hutchison, Avogadro: an advanced semantic chemical editor, visualization, and analysis platform, J. Cheminform. 4 (2012) 17, http://dx.doi.org/10.1186/1758-2946-4-17.
[37] Analytica EBC, Method 7.7, α- and β-Acids in Hop Products by HPLC, J. Inst. Brew., 2012.
[38] C. Schulz, C. Chiheb, M. Pischetsrieder, Quantification of co-, n-, and ad-lupulone in hop-based dietary supplements and phytopharmaceuticals and modulation of their contents by the extraction method, J. Pharm. Biomed. Anal. 168 (2019) 124–132, http://dx.doi.org/10.1016/j.jpba.2019.02.022.
[39] A.C. Hoek, A.C.J. Hermans-Lokkerbol, R. Verpoorte, An improved NMR method for the quantification of α-acids in hops and hop products, Phytochem. Anal. 12 (1) (2001) 53–57, http://dx.doi.org/10.1002/1099-1565(200101/02).
[40] D. Intelmann, G. Haseleu, T. Hofmann, LC-MS/MS quantitation of hop-derived bitter compounds in beer using the ECHO technique, J. Agric. Food Chem. 57 (4) (2009) 1172–1182, http://dx.doi.org/10.1021/jf803040g.
[41] G. Hostnik, J. Tošović, S. Štumpf, A. Petek, U. Bren, The influence of pH on UV/Vis spectra of gallic and ellagic acid: A combined experimental and computational study, Spectrochim. Acta A 267 (2022) 120472, http://dx.doi.org/10.1016/j.saa.2021.120472.